Earth-Science Reviews 258 (2024) 104949

Contents lists available at ScienceDirect

Earth-Science Reviews

journal homepage: www.elsevier.com/locate/earscirev

Review Article

Overland flow resistance: A review

Alessio Nicosia [a], Francesco Giuseppe Carollo [a], Costanza Di Stefano [a], Vincenzo Palmeri [a,b], Vincenzo Pampalone [a,*], Vito Ferro [a,b]

[a] Department of Agricultural, Food and Forest Sciences, University of Palermo, Viale delle Scienze, Building 4, 90128 Palermo, Italy
[b] NBFC, National Biodiversity Future Center, 90133 Palermo, Italy

ARTICLE INFO

Keywords:
Soil erosion
Overland flow
Flow resistance
Hillslopes friction

ABSTRACT

Shallow water flows over rough natural hillslopes contribute to interrill erosion and floods. The friction factor, that describes the hydraulic resistance, is particularly important for modeling soil erosion and transport processes. The present review focuses on the Darcy-Weisbach friction factor f for both large and small-scale roughness conditions and addresses the effects of rainfall intensity, vegetation cover, and sediment transport on overland flow resistance. All the studies on rainfall effect agree regarding the increase of the friction factor with rainfall intensity for the laminar flow regime and their independence for flows characterized by Reynolds number higher than a threshold varying between 800 and 2000. The analysis of the literature allows for concluding that f always increases with vegetation cover. Moreover, f (or its component due to sediment transport) increases with sediment concentration, slope, and Reynolds number, while it decreases with increasing values of Froude number and dimensionless sediment diameter. Finally, the focus areas for future research are highlighted.

1. Introduction

Water erosion on hillslopes is often a severe problem that causes economic and ecological damage. Soil loss from hillslopes is mainly ascribable to channelized (rill and gully erosion) and interrill (sheet erosion) erosion. Interrill erosion is caused by particle detachment due to rain splash and sediment transport by overland flow from interrill areas to rills (Mutchler and Young, 1975; Abrahams et al., 1994; Toy et al., 2002). Therefore, modeling soil erosion and transport processes at the hillslope scale needs the study of overland flow, which is characterized by a low water depth h, over a rough steep surface under the impact of rainfall. These characteristics make the measurements of flow depth and velocity difficult and lead to relatively large measurement errors (Govers et al., 2000).

To point out the effect of the rainfall impact, Emmett (1970) defined this flow type as "disturbed laminar flow". Considering that the overland flow is fed by rainfall and is subjected to infiltration losses that vary with time and location, it is both unsteady and spatially varying. In other words, for a given event with a constant rainfall intensity I higher than soil field-saturated hydraulic conductivity, according to the Hortonian scheme, runoff formation and the consequent transfer occur only for longer durations than ponding time. Besides the ponding time, a stationary condition is achieved when rainfall excess, equal to the difference between I and the soil infiltration capacity, does not vary. In this condition, in which it is possible to consider only the variation of the variables across the hillslope, the stationary flow increases depth in the flow direction due to runoff accumulation. Even if the rate of increase in water depth diminishes downward, and consequently the water surface tends to be parallel to the hillslope (considered as a uniform slope) asymptotically, the flow can be considered uniform because of the low water depth variability.

There are three widely-used empirical equations to predict the mean flow velocity V (m s^{-1}) (Darcy-Weisbach, Chezy, and Manning equations) in runoff and soil erosion models (Smith et al., 2007). Changing the hydraulic radius R (m) to the water depth h (m), as is common for overland flow whose width is usually much greater than flow depth, the hydraulic resistance can be evaluated through the Darcy-Weisbach friction factor f expressed as follows:

$$f = \frac{8ghs}{V^2} \tag{1}$$

in which g (m s^{-2}) is the gravitational acceleration, and s is the slope (−). For overland flow, the Reynolds number $Re = V h/\nu_k$ (or $= V R/\nu_k$ as $R \approx h$), where ν_k is the water kinematic viscosity, generally corresponds to

* Corresponding author.
E-mail address: vincenzo.pampalone@unipa.it (V. Pampalone).

https://doi.org/10.1016/j.earscirev.2024.104949
Received 2 February 2024; Received in revised form 23 July 2024; Accepted 30 September 2024
Available online 3 October 2024

the laminar regime but the flow cannot be considered as such because of the impact of the rainfall and the slope surface irregularities. For overland flow over a natural hillslope, Horton (1945) postulated the occurrence of a mixed flow regime, where areas with fully turbulent flow exist next to areas where the flow is laminar.

For turbulent flow, the relationship between unit width discharge q ($m^2\ s^{-1}$) and the water depth can be deduced from Eq. (1):

$$q = Vh = \left(\frac{8ghs}{f}\right)^{\frac{1}{2}} h = \left(\frac{8gs}{f}\right)^{\frac{1}{2}} h^{\frac{3}{2}} \tag{2}$$

For a given slope, and the assumption that f is almost constant, Eq. (2) states that the specific discharge is proportional to the 1.5 power of water depth. For laminar flow, the application of Poiseuille's law (De Marchi, 1977) leads to the following relation:

$$q = \left(\frac{gs}{3\nu_k}\right) h^3 \tag{3}$$

in which, for a given slope, q is proportional to the third power of h. Finally, Eqs. (2) and (3) can be expressed by the following general relation:

$$q = Ah^M \tag{4}$$

in which A is a proportionality constant and M is an exponent varying with the degree of flow turbulence from 1.5 (fully turbulent) to 3 (laminar). The comparison between Eqs. (2) and (3) indicates that, for a certain increase in discharge, the water depth increases more for turbulent than laminar flow. For mixed natural flows, as postulated by Horton (1945), the M exponent should vary from the two above limits.

The overland flow resistance can be affected by many factors, such as the bed roughness, rainfall impact, vegetation, and sediment transport, and has been investigated by laboratory and field experiments. Many authors, especially in the last decades (Fig. 1), carried out experiments to investigate different controls of overland flow resistance. The interaction between flow, bed morphology, and erosion can influence soil surface evolution and the mean velocity (Nearing et al., 2005). To demonstrate this hypothesis, Nearing et al. (2017) carried out six experiments with simulated rainfall (I = 59 and 178 mm h^{-1}) using 2 m × 6 m plots with three different slopes (5, 12, and 20 %) and initial rock cover ranging from 16 to 40 %. The soil surface evolution during the runs resulted in higher physical and hydraulic roughness for steeper slopes compared to the shallower ones. Furthermore, on the steeper slopes, the increase in roughness counterbalanced the increase in flow velocity. Nearing et al. (2017) explained this result by the so-called slope-velocity equilibrium, which expresses the roughness change over time due to the interaction between soil surface morphology and overland flow. This result can be assimilated to the feedback mechanism hypothesized by Govers (1992) (Palmeri et al., 2018; Carollo et al., 2021) for rill flows and used to explain the independence between slope and mean flow velocity.

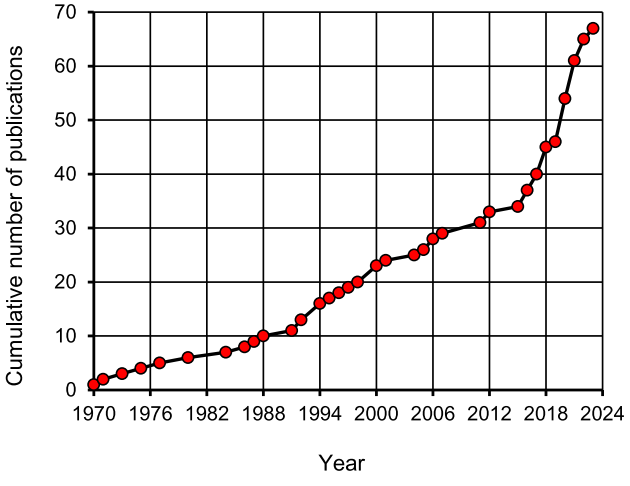

Fig. 1. Cumulative number of publications on overland flow resistance in the period 1970–2023.

The present review first focuses on the available f estimation models, and then addresses the effects of rainfall intensity, vegetation cover, and sediment transport on overland flow. The latter are widely dealt and, in many cases, framed into the presented models. Finally, research needs on overland flow resistance are also highlighted.

2. Friction factor models

2.1. f-Re power relationships

The effect of bed surface roughness on overland flow was investigated using both smooth and rough beds. For a sloping smooth/rough bed, the total flow resistance is given by the sum of internal fluid resistance and frictional resistance at the channel boundary (Katz et al., 1995). When boundary roughness does not affect the flow (uniform laminar case), the latter is characterized by a linear variation of shear stress with the bottom distance and by a local velocity that is equal to zero at the boundary and increases parabolically to a maximum at the free surface (Yalin, 1977; Katz et al., 1995). From the integration of the parabolic velocity distribution, Yalin (1977) obtained the following expression of the mean velocity V:

$$\frac{V}{u_*} = \frac{1}{3}\frac{u_* h}{\nu_k} \tag{5}$$

where $u_* = \sqrt{g R s}$ is the shear velocity.

If both sides of Eq. (5) are multiplied by V/u_*, the following theoretical relationship of the friction factor $f = 8\ u_*^2/V^2$ is obtained (Yoon and Wenzel, 1971; Yalin, 1977; Katz et al., 1995):

$$f = \frac{K}{Re} \tag{6}$$

where K is a constant. A more general form of Eq. (6) was suggested by Savat (1980) and Roels (1984):

$$f = \frac{K}{Re^{b1}} \tag{7}$$

where the b_1 exponent is equal to 1 for laminar flows (Eq. (6)) and is equal to 0.25 for turbulent flows. The K coefficient is equal to 24 for uniform flow on a smooth bed (Yoon and Wenzel, 1971) whereas it increases with increasing the slope gradient, flow depth and surface roughness (Phelps, 1975; Savat, 1980). Eq. (6) fitted well the data by Wang et al. (2019) collected in a 0.6-m-wide flume with a fixed bed with water depths ranging from 0.2 to 0.6 mm, slopes s ranging from 5.2 % to 25.9 % and bed roughness height k_s ranging from 0.009 to 0.380 mm. The increased K values for more rough conditions were explained as a result of the rolling waves and the increased water depth, which led to a greater contact area between the flow and sidewalls. Moreover, the viscous sub-layer cannot overlay the bed roughness as it increases. Therefore, as the rough elements extend into the mainstream, the streamlines deviate and the flow path length increases. In other words, the water flow is more chaotic, and f increases. Li et al. (2022) carried out flume experiments using water only and water-glycerol mixtures to obtain low Reynolds numbers, and k_s = 0.08, 0.18, and 0.38 mm. The analysis by Li et al. (2022) revealed that the flows with a water-glycerol mixture were always laminar, while the transition from a laminar to a turbulent flow regime for water-only flows occurred at Re = 500. The authors confirmed the applicability of the b_1 values suggested in the literature (b_1 = 1 for laminar flows and b_1 = 0.25 for turbulent flows),

while optimized the K coefficient. For laminar flow and the less rough surface ($k_s = 0.08$ mm), the K coefficient was close ($K = 28$, water only) or far ($K = 5.5$ water-glycerol mixture) from the theoretically-derived value of 24 for uniform flow on a smooth bed. In addition, it increased with surface roughness regardless of fluid type and flow regime.

Summarizing, the b_1 coefficient of Eq. (7) depends on flow regime, while K is affected by surface roughness, slope gradient, and flow depth. The K coefficient is also influenced by rainfall intensity as reported below in the specific section.

2.2. Lawrence models

Lawrence (1997) proposed to model the hydraulics of overland flow on rough granular surfaces using the inundation ratio $\Lambda = h/k_s$, rather than Re, as the primary control of flow resistance. With respect to the values of Λ, Lawrence (1997) identified three different overland flow regimes:

i) $\Lambda > 10$, the roughness elements are very small compared to the flow depth and constitute a boundary roughness that does not disturb the entire velocity profile. This condition of small–scale roughness corresponds to the well-inundated flow regime;
ii) $1 < \Lambda < 10$, the elements are inundated but exert a disturbing action on the entire velocity profile. This condition corresponds to the marginally inundated flow regime;
iii) $\Lambda < 1$, the elements protrude through the flow and induce both changes in the flow resistance and flow depth, and in the hydraulic radius, such that flow cannot be modeled as a broad shallow sheet flow. This condition corresponds to the partially inundated flow regime.

The second and third flow regimes correspond to large-scale roughness conditions. In the first case, which is analogous to the 'rough flow' regime in open-channel flow hydraulics, the relationship of the friction factor against the inundation ratio is deduced by adopting a logarithmic vertical velocity profile that, by integration, yields a semi-logarithmic resistance law. In the second regime, the flow can be modeled as a one-dimensional turbulent flow, even though the vertical velocity component due to the diversion of flow over roughness elements retards the downstream flow and thus contributes to additional resistance.

Lawrence (1997) proposed to apply Prandtl's mixing-length theory using a mixing length, l, proportional to the product between k and k_s, where $k = 0.4$ is the von Karman's constant. From this mixing length definition, the turbulent shear stress expression, and a linear distribution of the shear stress through the flow depth with the maximum at the bottom and null value at the free surface, a velocity distribution is obtained by integration. The further integration of this distribution yields the mean velocity and the following expression of the friction factor:

$$f = \frac{50\,k^2}{\Lambda^2} \approx \frac{10}{\Lambda^2} \tag{8}$$

For the partially inundated flow regime, the effect of each roughness element on the flow resistance becomes apparent and can be represented by the drag force, F_D, that depends on the drag coefficient of the element C_D, V, and the projected frontal area impacted by the flow A_F. Considering the number of elements per unit bed area, n_b, and applying the principle of superposition of effects for the computation of the total drag force, the effective boundary shear stress follows as $n_b F_D$. Under the hypothesis of a bimodal distribution of hemispheric particle sizes and larger hemispheres with radius equal to k_s, n_b is equal to $P/(\pi\,{k_s}^2)$, where P is the percentage cover, i.e., the percentage of the bed occupied by the larger elements. Combining the expressions of f, the effective boundary shear stress, and n_b, Lawrence (1997) proposed the following resistance law:

$$f = \frac{8}{\pi} P C_D min\left(\frac{\pi}{4}, \Lambda\right) \tag{9}$$

where min indicates the minimum value between $\pi/4$ and Λ. Even though not explicitly stated by the author, the *min* function should derive from exactly computing A_F for $\Lambda = 1$ ($A_F = 0.5\,\pi\,k_s^2$) and limiting A_F overestimation with the approximated relationship ($A_F = 2\,k_s\,h$) applied for the partial submergence condition, i.e., $\Lambda < 1$. The model by Lawrence (1997), which distinguishes three flow regimes and evaluates the friction factor based only on the degree of inundation, was positively tested against 1098 field and laboratory data points available from different investigations performed without rainfall and with a bed roughness mainly determined by grain roughness or, if it was the case, with a negligible effect of the vegetation. Overall, the agreement between the model and data was quite good, despite the data heterogeneity due to different experimental settings and techniques. Furthermore, it confirmed the generally non-monotonic relationship between the friction factor and the inundation ratio predicted by the model. This nonmonotonic f variation with increasing flow depth in the presence of macro-scale roughness was also recognized in other investigations (e.g., Abrahams et al., 1986; Ferro, 2003).

The results by Lawrence (1997) confirmed the goodness of the inundation ratio to determine the dominant physical mechanism controlling the friction mechanism, and the significant influence of the Reynolds number on flow resistance only for well-inundated flows at low to moderate Re values. However, the latter are quite rare in natural environments and less important, accordingly.

The model by Lawrence (1997) did not fit the data of Takken and Govers (2000) for partially inundated soil surfaces resembling a seedbed with different roughness. The authors attributed this result to the more complex roughness that cannot be characterized by a single measure of submergence, as in the model by Lawrence (1997).

The experiments carried out by Lawrence (2000) using plastic hemispheres and 10, 18, and 39 % percentage cover highlighted the need to correct the model for flows over partially inundated surface roughness accounting for the hydrostatic wave drag estimated from the free surface deformation around elements, i.e., wave resistance. Moreover, the author proposed a mixing length model that reflects the mathematical form of Eq. (8) and includes a roughness height scaling coefficient, C_s, and the percentage cover P resulting in:

$$f \approx \frac{10 C_s}{\Lambda^2} P \tag{10}$$

For partially inundated regime, the actual variable affecting flow resistance is the portion of the element height impacted by the flow. Consequently, the length scale k_s must coincide with h, and then $\Lambda = 1$. In other words, in this regime, Eq. (10) applies with $\Lambda = 1$. The value of $C_s = 0.78$ allowed the model to represent the experimental friction factor values for marginally inundated flows. Eq. (10) demonstrates that, for the investigated range of $10 \le P \le 39$ %, flow resistance increases with the percentage cover.

Mügler et al. (2011) performed high-resolution velocity measurements on a 10 m × 4 m rainfall simulation plot with a 1 % slope and sandy soil and assessed four different roughness models: a constant f value, the Lawrence (1997) model (including Eqs. (8) and (9)), a constant Manning coefficient n, and the expression by Jain et al. (2004) of n in which it decreases with increasing flow depth. Both the latter and the Lawrence model were calibrated by the available measurements. Based on the root mean square error quantifying the agreement between the simulated and the measured velocities, the best roughness model was that by Jain et al. (2004), followed by that of Lawrence (1997), the constant Manning coefficient, and the constant Darcy-Weisbach friction factor.

2.3. Theoretical approach

The dimensional analysis and self-similarity theory (Barenblatt, 1979, 1987) can be usefully employed to theoretically deduce the following flow velocity distribution in a uniform turbulent open channel flow (Ferro, 2017, 2018):

$$\frac{v}{u_*} = \Gamma\left(\frac{u_* y}{\nu_k}\right)^{\delta} \tag{11}$$

in which v is the local velocity, y is the distance from the bottom, $\delta = 1.5/\ln Re$ (Castaing et al., 1990; Barenblatt, 1991), and Γ is a function to be defined by velocity measurements. Integrating the power velocity distribution (Eq. (11)), the following expression of f can be obtained (Barenblatt, 1993; Ferro, 2017; Ferro and Porto, 2018):

$$f = 8\left[\frac{2^{1-\delta}\,\Gamma\; Re^{\delta}}{(\delta+1)\,(\delta+2)}\right]^{-2/(1+\delta)} \tag{12}$$

Setting $y = \alpha\, h$ the distance from the bottom at which the local velocity is equal to the cross-section average velocity V, from Eq. (11) the following expression of Γ is obtained (Ferro, 2017):

$$\Gamma_v = \frac{V}{u_*\left(\frac{u_*\alpha\, h}{\nu_k}\right)^{\delta}} \tag{13}$$

in which α is a coefficient < 1, considering that both V is located below the water surface and a single velocity profile is considered for representing the velocity distribution across the whole cross-section.

The following equation for calculating α was theoretically deduced (Ferro, 2017):

$$\alpha = \left(\frac{2^{1-\delta}}{(\delta+1)(\delta+2)}\right)^{\frac{1}{\delta}} \tag{14}$$

The theoretical flow resistance equation (Eq. (12) was applied to model stream (e.g., Ferro, 2017), rill (e.g., Di Stefano et al., 2022), and overland flows. Specifically, both plot and flume measurements from different overland flow investigations were used for the calibration of the following relationships (Eq. (15): Nicosia et al., 2020a, 2020b; Di Stefano et al., 2020; Nicosia et al., 2021a, 2021b; Eq. (16): Di Stefano et al., 2020; Eq. (17): Nicosia et al., 2020b, 2020c; Nicosia et al., 2021a; Eq. (18): Nicosia et al., 2021b; Nicosia et al., 2022 with $d = 0$):

$$\Gamma_v = \frac{a\, F^b}{s^c} \tag{15}$$

$$\Gamma_v = \frac{a\, F^b C_m^d}{s^c} \tag{16}$$

$$\Gamma_v = \frac{a\, F^b}{s^c Re_i^e} \tag{17}$$

$$\Gamma_v = \frac{a\, F^b}{s^c C_m^d Re^m} \tag{18}$$

where a, b, c, d, e, and m are positive calibration coefficients, $F = V/(gh)^{0.5}$ is the Froude number, which also accounts for the inundation ratio h/k_s (Ferro, 2018), C_m is the volumetric mean concentration of the sediment-laden flow, $Re_i = I\, h/\nu_k$ is a particular Reynolds number, named *rain Reynolds number*, where the rainfall intensity I is used in place of V.

Li et al. (2022) also positively tested Eqs. (12) and (18) with $d = 0$ and $m = 1$. Specifically, Eq. (18) was separately calibrated for water-only flows, mixed fluid flows with $Re < 7$, and mixed fluid flows with $Re \geq 7$. This threshold Reynolds number accounted for the different shape of the velocity profile, expressed by the exponent δ of Eq. (11), which is a function of Re. In fact, for $Re < 7$, the shape was estimated to be frequently linear ($\delta = 1$) or convex upward ($\delta < 1$), while for $Re \geq 7$, it was always concave upward ($\delta > 1$).

3. Effects of rainfall intensity

All the available literature studies (Table 1) agree regarding the increase of the friction factor with rainfall intensity for the laminar flow regime and their independence for flows characterized by Reynolds numbers higher than a threshold varying between 800 and 2000. The friction factor always increases with roughness height, while it decreases as Re increases under laminar flow regime. Moreover, analyzing the experimental conditions (plot/flume width, type of bed, and flow source) and ranges of the main variables (I, Re, and s) explored in the literature investigations (Table 2), it emerges that only two studies were performed for slopes equal to or higher than 20 %.

3.1. Experiments on smooth beds

In this experimental condition, the research conducted by Yoon and Wenzel (1971) was pioneering. They performed experiments on a sloping (0.5 and 1 %) smooth bed flume with I = 13, 32, 95, and 381 mm h^{-1}. These experiments allowed for deducing the influence of Re on flow resistance in the range $191 < Re < 5700$, recognizing that the relationship between flow resistance and rainfall intensity is related to Re. In particular, when Re is higher than 2000, the effect of rainfall intensity on flow resistance is almost negligible, while for $Re < 2000$, flow resistance increases with rainfall intensity (Fig. 2). This result can be explained with the concept of momentum transfer, according to which the local flow velocity is retarded by rainfall, especially near the free surface and to a different extent depending on the hydraulic conditions. Indeed, if the raindrop fall direction is nearly normal to the water surface, the quote of raindrop momentum in the mean flow direction is negligible, and consequently, a part of the mean flow momentum is needed to accelerate the raindrop mass. The major transfer of flow

Table 1
Variation of the Darcy-Weisbach friction factor f (or Manning's n) for increasing values of the variables considered in the investigations mainly concerning the effects of rainfall intensity.

Authors	I	k_s	Re	h/D_{50}
Yoon and Wenzel (1971)	↗ for $Re < 2000$; negligible for $Re > 2000$			
Shen and Li (1973)	↗ for $Re < 2000$			
Savat (1977)	negligible for high Re and s values			
Katz et al. (1995)	↗	↗		
Nearing et al. (2017)	↗			
Nicosia et al. (2020a)	↗ for $Re < 2000$ and $I >$ critical value falling in the range 32–95 mm h^{-1}; negligible for $Re > 2000$			
Nicosia et al. (2020b); Nicosia et al. (2021a)	↗ for laminar flows			
Shen et al. (2021a)	↗ for $Re < 800$		↘ for $Re < 800$	
Shen et al. (2021a)	↗ for $Re < 1070$		↘ for $Re < 1070$	↘
Shen et al. (2023)	↗	↗	↘	

↗ =*increase;* ↘ = *decrease;* Re = Reynolds number; h = water depth; k_s = characteristic roughness length; D_{50} = median raindrop diameter.

Table 2
Experimental conditions and ranges of the main variables explored in the literature investigations.

Rainfall intensity

Authors	I (mm h^{-1})		Re		s (%)		w (m)	Bed	Flow source
	min	max	*min*	max	*min*	*max*			
Emmett (1970)	79	304	5	327	0.3	17	1.22	rough	rainfall simulation (rs)
Yoon and Wenzel (1971)	13	381	191	5700	0.5	1	0.91	smooth	rainfall simulation
Shen and Li (1973)	190	444	n.a.	n.a.	n.a.	n.a.	0.6	n.a.	rainfall simulation
Savat (1977)	60	60	n.a.	n.a.	n.a.	n.a.	n.a.	smooth	rainfall simulation
Katz et al. (1995)	41	115	n.a.	n.a.	4	8	1	rough	rainfall simulation
Nearing et al. (2017)	59	178	48	194	5	20	2	rough	rainfall simulation
Shen et al. (2021a)	40	120	233	1031	2	27	0.25	smooth	rainfall simulation
Shen et al. (2021b)	40	120	laminar	turbulent	5	12	0.25	smooth	rainfall simulation
Shen et al. (2023)	40	120	laminar	laminar	5	12	0.25	rough	rainfall simulation

Vegetation

Authors	I (mm h^{-1})		Re		s (%)		w (m)	Bed	Flow source
	min	*max*	*min*	*max*	*min*	*max*			
Emmett (1970)	178	216	7	374	3	33	2.1	rough	rainfall simulation
Weltz et al. (1992)	65	65	turbulent	n.a.	4	13	3.05	rough	rainfall simulation
Abrahams et al. (1994)	–	–	n.a.	n.a.	n.a.	n.a.	0.5–0.61	rough	inflow
Parsons et al. (1994)	80	80	0.2	1	12	15	0.5–3	rough	rainfall simulation
Pan and Shangguan (2006)	100	100	33	40	27	27	0.55	rough	rainfall simulation
Kim et al. (2012)	10	10	n.a.	n.a.	10	110	1	rough	rs + inflow
Ye et al. (2015)*	–	–	572	4515	11	18	0.5	rough	inflow
Pan et al. (2016)	30	90	30	1400	3	50	1	rough	rs + inflow
Zhao et al. (2016)	–	–	785	2354	16	16	0.5	rough	inflow
Ding and Li (2016)	–	–	328	1588	36	36	2	rough	inflow
Yang et al. (2017)	–	–	210	810	18	18	0.4	rough	inflow
Zhang et al. (2017)*	–	–	158	1259	3	21	0.3	rough	inflow
Polyakov et al. (2018)	60	181	23	709	4	40	2	rough	rainfall simulation
Zhang et al. (2018)*	–	–	n.a.	n.a.	0	3	0.4	rough	inflow
Wang et al. (2018a)	80	80	22	55	9	47	1	rough	rainfall simulation
Wang et al. (2018b)*	–	–	4400	11,200	0.1	0.1	0.3	rough	inflow
Sun et al. (2018)	30	90	200	770	18	36	0.5	rough	rainfall simulation
Zhang et al. (2020)	–	–	n.a.	n.a.	1	1	0.4	rough	inflow
Shang et al. (2020)*	–	–	200	5400	7	21	0.3	rough	inflow
Bond et al. (2020)	–	–	41	417	9	23	0.4	rough	inflow
Li and Pan (2020)	60	60	50	200	47	47	2	rough	rs; rs + inflow
Zhang et al. (2021)	–	–	1023	20,658	0	3	0.4	rough	inflow
Ding et al. (2021)	–	–	1100	4100	9	27	0.37	rough	inflow
Cen et al. (2022)*	–	–	262	2700	4	21	0.3	rough	inflow
Dan et al. (2023)*	90	90	30	34	27	27	1	rough	rainfall simulation

Sediment transport

Authors	I (mm h^{-1})		Re		s (%)		w (m)	Bed	Flow source
	min	*max*	*min*	*max*	*min*	*max*			
Hu and Abrahams (2004)	–	–	637	3137	5	10	0.4	mobile	inflow
Hu and Abrahams (2005)	–	–	4824	11,462	5	13	0.25	fixed	inflow
Hu and Abrahams (2006) (from Hirsch (1996)	–	–	507	7095	11	11	0.5	large scale roughness	inflow
Hu and Abrahams (2006) (from Abrahams et al. (1991)	–	–	511	4347	11	11	0.4	large scale roughness+ rough+mobile	inflow
Abrahams and Parsons (1991)	–	–	100	1000	2	9	0.61	large scale roughness+ rough+mobile	inflow
Zhang et al. (2011)	–	–	414	3302	9	42	0.4	fixed rough	inflow
Ali et al. (2012)	–	–	55	1624	5	18	0.5	mobile rough	inflow
Liu et al. (2020)	–	–	613	6120	5	27	0.37	fixed rough	inflow

w = plot/flume width; – = not applicable; n.a. = not available. The Reynolds number Re is calculated as or is approximately equal to (for $R \approx h$) $Re = Vh/\nu_k$. The studies for which R is different from h ($Re = VR/\nu_k$) are identified by *.

momentum occurs in the proximity of the surface, and consequently, the velocity retardation diminishes from the surface downward. For a fixed rainfall intensity and drop size, the rate of raindrop impact does not change with Re, whereas the mean flow momentum increases, and the rate of momentum transfer decreases with increasing Re. The studies by Shen and Li (1973) and Savat (1977) confirmed the findings by Yoon and Wenzel (1971). Shen and Li (1973) carried out experiments on a smooth bed using a flume, 0.6 m wide and 18.3 m long, made of plexiglass walls and a stainless-steel bottom and I ranging from 190 to 444 mm h^{-1}. The authors highlighted that the flow Reynolds number and rainfall intensity affect flow resistance for Re less than 2000 and proposed the following estimate equation of the K coefficient of Eq. (6):

$$K = 24 + 27.16I^{0.407} \tag{19}$$

Savat (1977), using a single value of rainfall intensity (60 mm h^{-1}), found that the effect of rainfall diminishes for higher values of flow

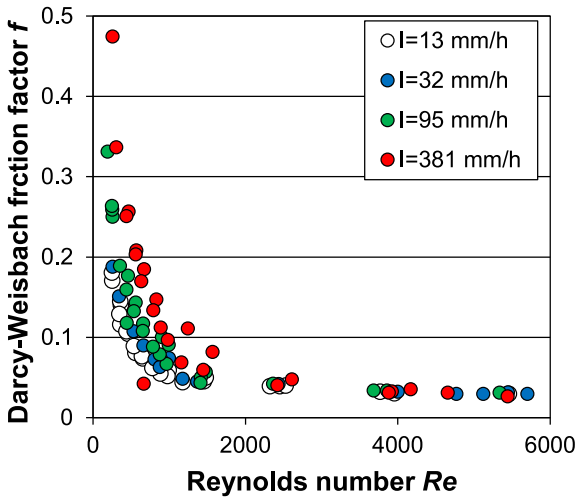

Fig. 2. Relationship between Re and f for the measurements by Yoon and Wenzel (1971).

turbulence or slope angle.

Recently, Nicosia et al. (2020a) successfully tested the applicability of Eqs. (12) and (15), where a, b, and c were expressed as linear functions of I, using the above-mentioned laboratory measurements by Yoon and Wenzel (1971). Moreover, they assessed the possibility of setting $I = 0$ mm h^{-1} into Eq. (15). Fig. 3a shows a good agreement between measured and estimated f values under the hypothesis $I = 0$ for $I \leq 32$ mm h^{-1}. For $I \geq 95$ mm h^{-1}, Fig. 3b highlights that this agreement is

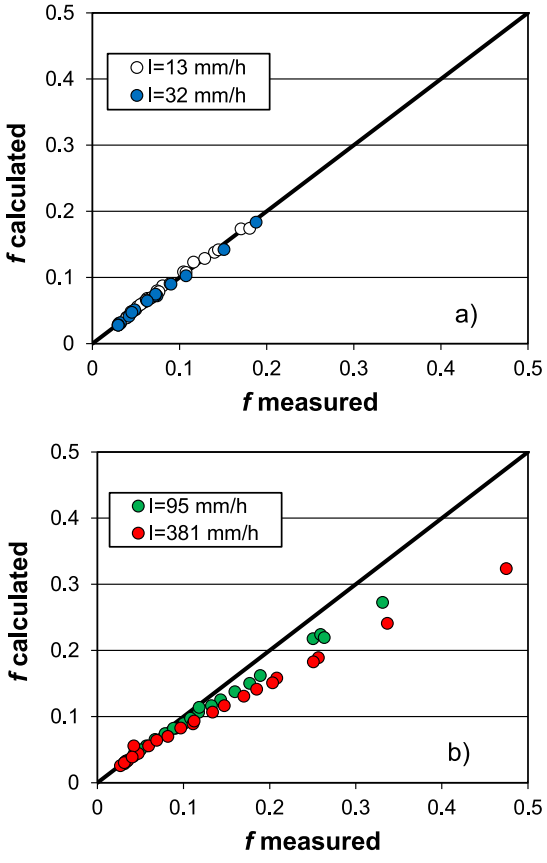

Fig. 3. Comparison between the measured and calculated values of the Darcy-Weisbach friction factor by Nicosia et al. (2020a) by setting $I = 0$ for $I \leq 32$ mm h^{-1} (a) and $I \geq 95$ mm h^{-1} (b).

confirmed only for $f \leq 0.06$–0.07. Considering that Re was always greater than 2000 for this specific range of f, the effect of I was always negligible for turbulent flows. On the other hand, since the estimated f values were systematically lower than the measured ones for $I \geq 95$ mm h^{-1} and $Re < 2000$, the analysis also showed that for $Re < 2000$, in the range 32–95 mm h^{-1}, a critical rainfall intensity can be detected, above which rainfall affects overland flow resistance and under which it does not significantly.

Recent studies (Shen et al., 2021a, 2021b) found different thresholds of Re to define the influence of rainfall intensity on flow resistance. Shen et al. (2021a) applied four simulated rainfall intensities ($I = 40$, 60, 100, and 120 mm h^{-1}) on a smooth flume (6.0 m long, 0.25 m wide, and 0.3 m deep) with a fixed bed and varying slopes (2–27 %). The flow regime was laminar with Re ranging from 233 to 1031. To study the effect of raindrop impact on flow resistance, half of the measurements were collected with the flume covered by a gauze screen near the runoff surface and half without. In this way, runoff was generated from rainfall only, i.e., without a base flow, in both cases and the effectiveness of the gauze screen in damping the rainfall kinetic energy was exploited to identify the rainfall effect by comparing the two measurement series. The results indicated that rainfall impact increased flow resistance and flow depth, and reduced flow velocity. The Darcy-Weisbach friction factor decreased in the slope range of 2–12 % and for $Re < 800$, while it was almost constant in the higher slope range and $Re > 800$. This Re value was found to separate laminar and turbulent flow regimes under rainfall conditions. The friction factor was modeled in the range $Re < 800$ by Eq. (7) with K proportional to $I^{0.086}$ and $b_1 = 0.907$ for the no gauze screening experiments, and K proportional to $I^{0.015}$ and $b_1 = 0.851$ for the gauze screening experiments. For $Re < 800$, the rainfall impact contribution to the flow resistance (Δf) was also expressed in the same mathematical form, reflecting that Δf decreases with increasing Re and increases with I.

Shen et al. (2021b) carried out two sets of experiments using the same flume and rainfall intensity values as Shen et al. (2021a). The runs were characterized by upstream inflow with rainfall and upstream inflow only, and three gentle slopes (5, 9, and 12 %). For the tests with upstream inflow only, f decreased with increasing flow depth. For Re values less than 1070, f decreased with increasing Re following the power Eq. (7) with $K = 34$ and $b_1 = 0.828$, while it was nearly constant for $Re > 1070$. For the upstream inflow with the rainfall tests, the rainfall intensity did not affect mean flow velocity significantly at different inflow depths. The friction factor decreased with increasing Re according to Eq. (7) and the additional effect of rainfall on the friction factor was apparent for $Re < 1070$ while declining over this threshold. The ratio between the flow depth h and median raindrop diameter, D_{50}, also affected the friction factor and gradually weakened with increasing values of this ratio. When the flow depth is deeper than three raindrop diameters, the impact force of raindrops is suppressed (Guy et al., 1987), but in the experiments by Shen et al. (2021b) h/D_{50} was less than three and the effect of rainfall did not vanish. The nonlinear regression analysis of the data yielded model f according to an equation that can reduce to Eq. (7) with $b_1 = 0.675$ and K proportional to $(h/D_{50})^{-0.542}\, s^{-0.119}$.

3.2. Experiments on rough beds

Katz et al. (1995) glued sand grains in a flume 4.87 m long and 1 m wide, where they performed experimental runs with three different slope values ($s = 4$, 6, and 8 %) and two simulated rainfall intensities ($I = 41$ and 115 mm h^{-1}). The K coefficient of Eq. (6) was higher than 24, which is the theoretical value for uniform flow on a smooth bed and can be considered representative of the combined effect of rainfall and bed roughness. Therefore, K depends on rainfall intensity and the characteristic roughness length k_s, which was set equal to the sand median diameter d_{50} (mm). The measurements allowed for determining the following relationship:

$$K = 24\left(\frac{d_{50}}{0.7}\right)^{2.16}\left(\frac{I}{40}\right)^{0.33} \quad (20)$$

which highlights that the K estimation is more affected by errors associated with the bed roughness evaluation (d_{50}) than those deriving from the uncertainty on the rainfall intensity.

The laminar flow measurements on a stony hillslope by Nearing et al. (2017) demonstrated that flow resistance increases with rainfall intensity, and the mean velocity is independent of the slope gradient. The related friction factor was well estimated by Eqs. (12) and (17) (Nicosia et al., 2020b) in which the rain Reynolds number accounts for the effect of rainfall intensity and allowed for improving the f estimate as compared with the combined use of Eqs. (12) and (15). Nicosia et al. (2021a) also calibrated Eq. (17) on the laboratory and field measurements carried out by Emmett (1970) for the laminar flow regime. The calibrated equation for laboratory data resulted in an increasing friction factor with rainfall intensity and was validated against the smooth bed data by Yoon and Wenzel (1971) to assess its applicability for different bed roughness conditions (Fig. 4). Fig. 4 shows the inapplicability of the equation calibrated for a rough bed condition to estimate f for a smooth bed condition under lower rainfall intensity and, conversely, the applicability for the higher rainfall intensities. Indeed, in the former case the rainfall effect is negligible (Nicosia et al., 2020a) and the bed roughness effect is dominant and cannot be neglected, while the opposite occurs in the latter case.

Shen et al. (2023) also performed several tests of rainfall (I = 40, 60, 100, and 120 mm h^{-1}) and inflow with surface roughness k_s ranging from 0.009 to 0.25 mm and a laminar flow regime, using the same flume as Shen et al. (2021a, 2021b) and slopes ranging from 5 to 12 %. Roughness had a positive effect on flow resistance both without and with raindrop impact, and rainfall increased f for all roughness values. The roughness contribution to the friction factor was higher than that (Δf) due to the rainfall impact. The friction factor decreased with increasing Re according to Eq. (7) with K and b_1 varying with the surface roughness. A non-linear regression analysis allowed the authors to elucidate that b_1 = 0.8 and K is proportional to $(k_s\, I)^{0.2}$. For F less than approximately 2, Shen et al. (2023) also proposed a predictive equation of Δf having the form of Eq. (7), b_1 = 1.5, and K proportional to $k_s^{0.3}\, I$. Both f and Δf were mainly affected by the Reynolds number. The findings by Shen et al. (2021a, 2021b) and Shen et al. (2023) are limited to the investigated fixed bed conditions.

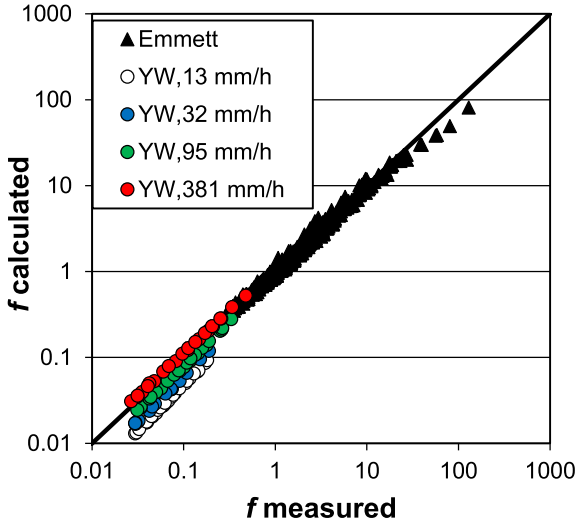

Fig. 4. Comparison between literature measurements of the Darcy-Weisbach friction factor and the calculated values by Nicosia et al. (2021a) (Eqs. (12) and (17)).

4. Effects of vegetation

The analysis of the available literature (Table 3) allows for concluding that flow resistance always increases with vegetation cover. Moreover, f diminishes with increasing values of the Reynolds number for sparse or absent vegetation, while it increases with Re for dense vegetation. This last result is common to different investigations, except for that by Zhang et al. (2021). From all the studies arose that the friction factor decreases primarily as the slope grows, while its relationship with rainfall intensity is controversial.

Table 2 highlights that most of the studies concerning the effects of vegetation on overland flow resistance were carried out using only inflow discharge, while the simultaneous application of simulated rainfall and inflow discharge as flow source is limited. This can be due to the circumstance that the effect of rainfall often becomes negligible for vegetated beds.

4.1. *Effect of vegetation type*

The experimental runs concerning the study of the effects of vegetation type on flow resistance were mainly performed under simulated rainfalls. Emmett (1970) carried out field experiments on sloping (3 to 33 %) plots with vegetation. Different rainfall intensities (from 178 to 216 mm h^{-1}) were reproduced by a rainfall simulator and the generated flows were laminar (Re varying from 7 to 374) and subcritical (F varying from 0.008 to 0.76). The results showed that vegetation and topographic irregularities greatly affect flow resistance on natural hillslopes, while the slope effect is negligible as compared to those of other variables.

The database published by Polyakov et al. (2018) was used by Nicosia et al. (2020c) to assess the applicability of Eqs. (12) and (17) for vegetated plots. The database consists of overland flow runs under simulated rainfalls with I in the range 60–181 mm h^{-1}. The experiments were performed at the Southwest Watershed Research Center of the USDA, on 2 m × 6 m plots located in 23 semiarid rangeland locations in Arizona and Nevada. The plots were characterized by great variability in terms of slopes and four different vegetation covers (Perennial grass, Shrub, Juniper, treated Juniper). For the tested laminar overland flows, the authors found that flow resistance increases with rainfall intensity and no relation between slope and mean velocity. Moreover, due to the laminar flow regime, the variations in flow resistance due to different vegetation types were negligible. To broad the range of subcritical flows and rainfall intensity examined by Nicosia et al. (2020c), Nicosia et al. (2021a) used the field runs by Emmett (1970). The data were used to calibrate Eq. (17) with b and c coefficients previously determined by Nicosia et al. (2020c) and attributing the effect of different types of vegetation to the a coefficient. The results confirmed that a was almost constant for the tested laminar flow regime.

Weltz et al. (1992) collected data from fourteen different native rangeland areas in the western United States, applying rainfall at a constant intensity of 65 mm h^{-1} from a rotating-boom rainfall simulator on runoff plots to estimate hydraulic roughness coefficients for overland flow by a subfactor-based regression technique. They evaluated different f subfactors using smooth bare soil, gravelly bare soil, and sparsely to densely vegetated rangeland areas (short-, mid-, and tallgrass prairies; desert shrubs and sagebrush; and oak and pinyon-juniper woodlands). Weltz et al. (1992) derived regression equations to predict an "effective Darcy-Weisbach roughness coefficient" for native rangeland which include the effects of raindrop impact, random roughness, rocks, litter, and canopy and basal plant cover, but they found no trend between the effective roughness coefficient and the type of vegetation (grass or shrub) or soil texture.

Li and Pan (2020) performed rainfall simulations in field plots (5 × 2 m^2) constructed on a loess hillslope (s = 47 %), including bare soil plot, as control, and three plots vegetated with forage species (*Astragalus adsurgens*, *Medicago sativa* and *Cosmos bipinnatus*). The results show that vegetation, on average, increased f by188% and decreased flow velocity

Table 3
Variation of the Darcy-Weisbach friction factor f (or Manning's n) for increasing values of the variables considered in the investigations mainly concerning the effects of vegetation.

Authors	Q	I	s	Re	d	Cover degree	lodging angle	F	h/H_v
Abrahams et al. (1994)				↘for shrubland;					
				↗for grassland					
Pan and Shangguan (2006)						↗			
Kim et al. (2012)	↗gentle slope;		↗low Q;			↗			
	↘steep slope		↘high Q						
Ye et al. (2015);						↗			
Zhao et al. (2016);									
Ding and Li (2016)									
Pan et al. (2016)			↗for grass						
Yang et al. (2017)				↘for non-vegetated;					
				↗for vegetated					
Zhang et al. (2017);				↘for low cover;					
Cen et al. (2022)				↗for high cover					
Zhang et al. (2018)			↘		↗				
Wang et al. (2018a)			↗			↗(litter)			
Sun et al. (2018)		↘	↘			↗			
Zhang et al. (2020)							↘		
Nicosia et al. (2020c)		↗							
Zhang et al. (2021)			↘	↗sparse		↗		↘	↗
Dan et al. (2023)				↘for bare soil;					
				↗for other treatments					

↗ = *increase;* ↘ = *decrease;* Q = flow discharge; s = slope; Re = Reynolds number; h = water depth; d = stem diameter; F=Froude number; h/H_v = vegetation submergence ratio.

by 30 %. Ferro (2020) used the data by Li and Pan (2020) for calibrating Eq. (17), with $c = 0$, obtaining that f can be reliably estimated and varies with rainfall intensity. This author also obtained that the vegetation type does not significantly affect flow resistance for the investigated laminar regime, confirming the results by Nicosia et al. (2020c).

Another investigation was conducted by Sun et al. (2018) on forest-covered slopes with two different treatments (vegetation and vegetation with litter) for different combinations of rainfall intensities (30, 60, and 90 mm h^{-1}) and slope gradients (18, 27, and 36 %). They found that f decreased for increasing rainfall intensity and slope gradient, and litter layer increased f by three to nine times.

Dan et al. (2023) performed flume experiments with simulated rainfall and four different cover treatments (i.e., bare soil, grass cover, biological soil crust (BSC), and grass cover with BSC) to also study the variations in friction factor. The f value decreased with increasing Re on bare soil slopes, while it increased with increasing Re for the other treatments, as water turbulence and water depth increased, and BSC and grass constituted protruding elements determining additional flow resistance.

Other experiments involving the study of how vegetation type influences flow resistance were carried out using inflow discharge as a flow source instead of simulated rainfall.

Abrahams et al. (1994) carried out 136 experiments on semiarid grassland and shrubland hillslopes at Walnut Gulch, Arizona, on plots where runoff was generated by flow onto the upper end of the plots from a trickle pipe. The relationship between f and Re was positive for the grasslands and negative for the shrubland. They attributed these contrasting results to the progressive inundation of the roughness elements, with the submergence of the gravel on the shrubland being greater than the submergence of the plants on the grassland. Abrahams et al. (1994) found higher flow resistance on grassland than shrubland and derived multivariate models including surface properties among the predictive variables for the grassland and shrubland hillslopes. They stated that on the grassland 70 % of the variation in f is due to basal plant stem and litter cover, whereas on the shrubland 56 % of the variation is explained by gravel cover and gravel size. The authors suggested that including Re slightly (5 % on the grassland and 7 % on the shrubland) improves the accuracy of the flow resistance estimate and that, consequently, the

practice of estimating it only by surface properties is entirely reasonable. The experiments undertaken on grassland plots by Parsons et al. (1994) were conceived to explain the differences between f values obtained by Weltz et al. (1992) (rain-induced overland flow) and Abrahams et al. (1994) (trickle-induced flow) for similar plots within the Walnut Gulch experimental watershed. The analysis by Parsons et al. (1994) demonstrated that the friction factors of rain-induced overland flows are approximately an order of magnitude greater than those for trickle-induced overland flow. Considering these marked differences and that rain-induced overland flow reproduces runoff under natural rainfall better than trickle-induced flow does, the authors suggested that f predictive equations are best determined under rain-induced overland flow.

Bond et al. (2020) performed velocity measurements for four upland grassland habitats (Rank Grassland, Low-density Grazing, Hay Meadows and Rushes) using a portable hillslope flume (0.4 m large and 2 m long), and applied three flow discharges (1, 6, and 12 L min^{-1}) during five campaigns in April, June, July, September, and November 2019, in sampling locations characterized by slope values ranging from 9 to 23 %. The results showed that seasonal vegetation change should be incorporated into flood modeling, as cycles of surface roughness in grasslands strongly modify overland flow, having a potential impact on downstream flood peak and timing. Ferro and Guida (2022) calibrated Eq. (18) with the coefficient $d = 0$ using the measurements carried out by Bond et al. (2020). The calibration was made specifically for each upland grassland type and the phases of vegetation growth. Eqs. (12) and the calibrated Eq. (18) allowed for an accurate estimation of the Darcy-Weisbach friction factor. Moreover, f was slightly affected by the seasonal variation of roughness in these grassland environments.

Finally, the contemporary application of both flow sources (i.e., simulated rainfall and inflow) characterizes the experiments by Pan et al. (2016) on granular surfaces (bare soil and sandpaper) and grassed surfaces (grass plots (GP), GP with litter, and GP without leaves). The runs were performed for $30 < Re < 1400$ and slopes varying from 3 % to 50 %. The authors observed a good f-Re relation (Eq. (7)) for granular surfaces, and a good relation between f and F for grass plots. Pan et al. (2016) detected a non-monotonic pattern between f and slope for the granular surface with higher f at the gentle and steep slopes. Conversely, the friction factor decreased with increasing slopes for the grass treatments, demonstrating that f is not a simple function of slope. The authors obtained values of the contribution of grass leaves, stems, litter, and grain surface to total resistance in the grass plots on average equal to 52 %, 32 %, 16 %, and 1 %.

The above mentioned study by Li and Pan (2020) also included inflow addition to the rainfall-induced flow. Vegetation, constituted of forages, increased f on average by 202 % compared to the bare soil condition, which expresses a more remarkable effect of vegetation compared to the only rainfall condition (average f increase of 188 %).

4.2. Effect of vegetation cover degree

The studies regarding the effects of vegetation cover degree on flow resistance were predominantly carried out using inflow discharge as a flow source. Only two studies (Pan and Shangguan, 2006; Wang et al., 2018a) were performed with rainfall simulation.

Pan and Shangguan (2006) performed laboratory experiments on plots covered by grass (35 %, 45 %, 65 %, and 90 % cover) and a bare soil plot, as a control, at a slope of 27 %. They found that, for increasing grass cover, f increased and velocity decreased with a more significant reduction downslope than upslope. Pan and Shangguan (2006) also found that f increased with increasing grass cover.

Wang et al. (2018a) performed simulated rainfall experiments on five slope gradients (9, 18, 27, 36, and 47 %) with an extreme rainfall intensity of 80 mm h^{-1} and using six litter covers (0, 0.05, 0.10, 0.20, 0.35, and 0.50 kg m^{-2}) and four litter types (deciduous trees, coniferous trees, shrubs, and herbs), which were incorporated into topsoil. The results pointed out that the Froude number and flow velocity decreased, while flow resistance increased drastically with litter cover. Wang et al. (2018a) found that litter type influenced flow hydraulics, due to the variations in surface cover of the exposed litter and the litter morphology. According to the obtained results, V and f considerably increased with s. However, the change in slope gradient did not influence the relationships between flow hydraulics and litter rate. Finally, the authors found a linear trend between the random roughness, resulting from heterogeneous erosion due to the uneven protection of surface exposed litter, and litter incorporated rate.

Ding and Li (2016) conducted laboratory scouring experiments to investigate the influence of grass cover on runoff, erosion rates, and overland flow hydraulic characteristics in plots at a slope gradient of 36 % with different grass cover rates (30, 50, 70, and 90 %), grass distribution patterns (grass laid on upslope, middle-slope, and down-slope) and with a bare soil. For these experiments, Re varied from 328 to 1588, while F fell in the range 0.23–1.97. The overland flow velocity increased with increasing inflow and linearly decreased with increasing grass cover. The average f of the whole slope for grass plots was 2.2–25.6 times that for bare soil plots, and f was related to the cover rate.

Zhang et al. (2017) performed flume (6.0 m long, 0.3 m wide, and 0.25 m deep) experiments with six slopes (in the range 3–21 %), seven flow discharges, and five degrees of vegetation cover (no cover, 2, 5, 7, and 9 %). For low vegetation cover, f decreased with increasing h and Re values, while the opposite pattern occurred for high vegetation covers. The pattern inversion occurred for a vegetation cover of 5 %. Zhang et al. (2017) also proposed equations for predicting V and f depending on the vegetation cover percentage, which, however, did not give accurate estimates of the considered variables as the coefficient of determination was equal to 0.63 and 0.43, respectively.

Another investigation on runoff hydraulics was carried out by Shang et al. (2020) on slopes inclined from 7 to 21 % and covered with wheatgrass patches with vegetation density of 0.6 % to 5.8 %. Hypothesizing that the total resistance can be divided into a vegetation component and a grain component, they observed that increasing density vegetation changes the former component from 95 % to 99 % of the total resistance and highlighted that vegetation is the most significant tool in soil erosion control.

4.3. Effect of stem vegetation

The effect of stem vegetation on flow resistance has been largely investigated using inflow discharge as a flow source. Ye et al. (2015) performed experiments for smooth, sand, and vegetated (with *Chlorophytum malayense* or *Ophiopogon bodinieri*) flumes. Moreover, both aligned and staggered vegetation configurations were tested. The authors found that, for all the rough beds and configurations, f decreased with increasing unit flow rate and tended to a constant value for a unit flow rate of 3 L s^{-1} m^{-1}, associated with $F = 1$ and $Re = 4000$. Ye et al. (2015) also found that the flow behavior was less influenced by the configuration than density of vegetation, and a lower vegetation density reduced flow resistance. For laminar flows, the authors determined a K value (Eq. (6)) of 5000, much higher than that (24) on smooth beds.

Zhao et al. (2016) carried out laboratory experiments on a sloping (16 %) flume to investigate the potential effects of rigid vegetation stems on Re (varying from 785 to 2354, calculated considering the whole flume section), F (varying from 0.77 to 3.29), V, and hydraulic resistance of silt-laden overland flow. The stems were simulated by cylinders with different diameters (2, 3.2, and 4 cm) glued onto the flume bed with a triangular pattern, and a bare slope was used as a control. These authors obtained that the Reynolds number on the vegetated slope was significantly higher than that on the bare slope due to the effect of vegetation stems on effective flow width. For all the examined flows, the Froude number decreased with increasing cylinder diameter. The Darcy-Weisbach friction factor increased for higher diameters, implying that the energy consumption of overland flow increased due to the wider area occupied by the cylinders. Zhao et al. (2016), investigating the

contribution to total flow resistance on vegetated slopes due to grain resistance and vegetation resistance, found that the latter accounted for almost 80 % of the total resistance and was the dominant roughness element. Since the flume used by Zhao et al. (2016) was smooth and the experiments were carried out for a sediment-laden flow, the so-called grain resistance probably referred to the contribution due to transport phenomena to flow resistance.

Yang et al. (2017) carried out experimental runs in a sloping flume (5.2 m long, 0.4 m wide, and 0.1 m high) using circular cylinder rods with different diameters simulating rigid vegetation with three different vegetation densities (1.7 %, 3.5 %, and 6.1 %). The flume bed was covered by sandpaper, simulating three different surface roughness values. The authors found a negative correlation between the hydraulic resistance and Reynolds number on non-vegetated slopes, and the opposite trend on the vegetated ones. The authors, applying the additive method of flow resistance, found that the surface roughness has greater influence on overland flow resistance than vegetation stem for low unit discharges, while the vegetation effect is dominant for high unit discharges. Yang et al. (2017) also found that the combined effects of the two components (simulated vegetation and surface roughness) differ from the sum of the individual effects.

Zhang et al. (2018) carried out an experiment using three different slope gradients, three vegetation stem diameters, and twelve unit-discharge values to study the effect of vegetation stem diameter and slope gradient on overland runoff and flow resistance. These authors found that the diameter of the vegetation stem and the slope gradient have a significant resistance effect. Moreover, under the same slope gradient, f increased with an increase in the vegetation stem diameter (an increase in the diameter of 1 mm determined an average f increase of 50 %). Zhang et al. (2018) found that, for a given vegetation stem diameter and square vegetation distribution pattern, the greater the slope gradient, the smaller the value of f, and as the slope increased by 1 %, f decreased by an average of 25 %.

Wang et al. (2018b) conducted experiments through rigid emergent vegetation having three densities (dense, middle, and sparse) and positions (summit, backslope, and footslope). The authors found that the f vs. Re relationship was much less pronounced on vegetated slopes than bare ones, and Re was predictor of hydraulic roughness together with the tested experimental arrangements Moreover, the dense backslope arrangement was the optimal vegetation pattern to maximize flow resistance.

Zhang et al. (2020) conducted indoor experiments in a 5-m-long and 0.4-m-wide flume in which a Plexiglas board was placed at the bottom to simulate the underlying surface of vegetation planting characterized by different values of lodging angles (from 35 to 139 %), i.e., the angular difference between the stalk under the flow impact and its upright state. The Darcy-Weisbach friction factor gradually decreased with increasing lodging angle for a fixed water depth and all the degrees of vegetation submergence. For unsubmerged vegetation, Zhang et al. (2020) obtained that flow resistance increased with the water depth for a fixed lodging angle, while for submerged vegetation, they found an opposite trend. For both submerged and unsubmerged vegetation, they also provided quantitative formulas relating the lodging angle and f.

Zhang et al. (2021) studied overland flow resistance under sparse vegetative stem cover (fixed diameter equal to 4 mm). They carried out experiments under four slope gradients (0, 1 %, 2 %, and 3 %), seven flow discharges, and six degrees of vegetation cover (0.72, 0.37, 0.20, 0.13, 0.11, and 0.07 %) organized in a square pattern. Their results showed that the Manning coefficient changed with vegetation submergence, while the Reynolds number, Froude number, and slope were closely related to vegetation cover. Also, Zhang et al. (2021) found that the Manning coefficient is positively correlated to vegetation submergence, Reynolds number, and vegetation cover, while is negatively correlated to Froude number and slope. These authors found that vegetation cover is the dominant factor affecting overland flow resistance under zero-slope conditions, while the ratio h/H_v of water depth to the vegetation height H_v is the dominant factor, followed by vegetation cover and slope, under slope conditions.

Ding et al. (2021) carried out two series of flume experiments with three slope gradients (9 %, 18 %, 27 %) and three flow discharge rates (0.5, 1.0, 1.5 L s^{-1}), for testing the effects on hydraulic variables due to artificial Gramineae stems with a 0–30 % cover level and *Pinus tabulaeformis* litter with a 0–70 % cover level. The flow velocity and depth were measured by the electrolyte tracer technique and three-level probes, respectively. These authors observed that the Froude number and flow velocity affected by stem cover were much lower than those affected by litter cover, whereas the opposite trend was found for the Reynolds number, flow depth, and shear stress. Moreover, Ding et al. (2021) found that the form resistance caused by stems was 22–57 times greater than that caused by litter for the same cover level, suggesting that stem cover is a more efficient management option to increase the flow resistance and reduce flow capability for sediment detachment and transport. These authors also proposed new equations for calculating Manning's n and flow velocity under the influence of litter cover.

Cen et al. (2022) tested 30 vegetation configurations (combining 5 synthetic grass covers and 6 synthetic stem covers) applying five discharges on a sloping flume (four slope gradients varying from 4 % to 21 %). They observed that the relationship between f and Re depends on vegetation cover. In particular, according to the findings by Zhang et al. (2017), for increasing values of the vegetation cover, first f is negatively correlated with Re and then is positively correlated. The vegetation cover value which determines the inversion of the trend decreases for increasing slope gradients.

The only study for which a different flow source was used is that by Kim et al. (2012), who carried out overland flow simulations with a 1 m wide and 2 m long plane, using slopes ranging from 10 to 110 %. The experimental runs were performed with a simulated rainfall of 10 mm h^{-1} and inflow discharge, for non-vegetated conditions and with vegetation covers of 5, 10, 20, 30, and 50 % given by randomly located vegetation stems. The authors obtained that n grows for increasing vegetation cover values. Moreover, for fixed vegetation cover and discharge, they found a positive relationship between slope and n at low-flow rates, and a negative one at high-flow rates. For fixed vegetation cover and slope, Kim et al. (2012) found a positive relationship between the flow discharge and n for gentle slopes and a negative one for steep slopes. The authors also developed predictive equations for estimating n depending on Froude number, Reynolds number, slope, and vegetation cover density.

Table 4
Variation of the Darcy-Weisbach friction factor f (or its component due to sediment transport) for increasing values of the variables considered in the investigations mainly concerning the effects of sediment transport.

Authors	C_m	h/k_s	s	Re	F	ks_*
Hu and Abrahams (2004) (f_{btm})	↗	↗	↗		↘	↘
Hu and Abrahams (2005) (f_{mob})						↘
Nicosia et al. (2021b)	↗		↗	↗	↘	
Nicosia et al. (2022a)			↗	↗	↘	

↗ = *increase;* ↘ = *decrease;* C_m = volumetric sediment concentration; h = water depth; k_s = characteristic roughness length; s = slope; Re = Reynolds number; F=Froude number; k_{s^*} = dimensionless sediment diameter; f_{btm} = component of the friction factor due to bed-load transport resistance for mobile beds; f_{mob} = $f_{btm} - f_{btf}$, in which f_{btf} is the bed-load transport resistance for fixed beds.

5. Effects of sediment transport

Despite the limited number of investigations, the results are consistent regardless of the considered variable (Table 4). Specifically, f (or its component due to sediment transport) increases with sediment concentration, slope, and Reynolds number, while it decreases with increasing values of Froude number and dimensionless sediment diameter. However, Table 2 also shows that all the experiments concerning the effects of sediment transport on overland flow resistance were carried out using inflow discharge, whereas simulated rainfall and inflow discharge, which better mimic natural conditions, were never applied simultaneously.

To extend the study by Gao and Abrahams (2004), Hu and Abrahams (2004) performed 38 flume experiments on slopes of 5 and 10 %. They used mobile beds and sediment with median diameter k_s of 0.74 mm and 1.16 mm but scour or deposition of the bed was prevented. The study aimed to investigate the factors controlling the component f_{btm} of the friction factor f due to bed-load transport resistance. The values of f_{btm} were calculated as the difference between f and grain resistance, f_g, derived from the Savat's (1980) algorithm. The investigated flows were supercritical ($1.10 \leq F \leq 2.16$) and turbulent ($637 \leq Re\ (=Vh/\nu_k) \leq 3137$). Hu and Abrahams (2004) found that f_{btm} is mainly controlled by the volumetric sediment concentration C_m, inundation ratio h/k_s, and the dimensionless sediment diameter $k_{s*} = k_s\left[\left(\frac{\gamma_{s-\gamma}}{\gamma}\right)\frac{1}{\nu_k^2}\right]^{1/3}$, in which γ_s and γ are the sediment and water specific weight. Moreover, they identified the dependence of f_{btm} on F and s. These five factors were responsible for 97 % of the variance of f_{btm}, and s controlled it entirely through C_m, which was therefore redundant. Finally, the authors proposed a predictive relationship of f_{btm} with k_{s*}, h/k_s, s, and F as controls, which does not necessitate measuring bed-load transport rate:

$$f_{btm} = 267.3k_{s*}^{-1}\left(\frac{h}{k_s}\right)^{0.5}F^{-3}s^2 \tag{21}$$

where the numerical coefficients are fitting constants.

Hu and Abrahams (2005) carried out experiments using the same flumes as Hu and Abrahams (2004). They performed 54 fixed bed runs and, in addition, used the data by Hu and Abrahams (2004) from mobile bed runs. The median diameter k_s of the beds and sediment was 0.74 mm and 1.16 mm. The authors calculated f_{btm} and f_{btf} (bed-load transport resistance for fixed beds) from the difference between f and f_g estimated with the Savat (1980) algorithm, obtaining that, on average, the bed-load transport resistance accounted for one-quarter of the total flow resistance f. The component of the bed-load transport resistance due to bed mobility was $f_{mob} = f_{btm} - f_{btf}$, in which f_{btm} was estimated by Eq. (21) and f_{btf} by an equation similar to Eq. (21), where a term depending on the sediment concentration was in place of k_{s*}. The values of f_{mob} were always positive implying that mobile beds offer greater resistance to flow than fixed ones. The authors ascribed this result to grain collisions with mobile beds being less elastic than with fixed beds, which causes more momentum loss. Finally, f_{mob} was expressed as follows:

$$f_{mob} = 51.2k_{s*}^{-2.25}f^{0.75} \tag{22}$$

indicating that f declines as the grains are larger and thus less mobile, and that f_{mob}, as a component of f, covaries with f. On average, f_{mob} was approximately equal to half of f_{btm} and one-eighth of f.

Hu and Abrahams (2006), applying the additive method of shear stresses (Yalin, 1977), assumed a partition of flow resistance without rainfall into four components: grain resistance f_g, form resistance f_f, wave resistance f_w, and bed-mobility resistance f_m. Grain resistance depends on the nature of the surface in contact with the flow, form resistance is due to obstacles protruding into or through the flow, and wave resistance accounts for the free surface deformation around elements (Abrahams and Parsons, 1994; Lawrence, 2000). Bed-mobility resistance f_m is a comprehensive component of flow resistance with regard to the processes associated with a moving bed (e.g., bed-load transport, bed deformation, and bed elasticity), and differs from both f_{btm} and f_{mob}. Two series of literature data were used, featured by smooth fixed beds and rough mobile beds, respectively, over which cylinders with diameter D_r served as large-scale roughness elements. The hydraulics and bed roughness characteristics of the two series of experiments were similar and a single slope value of $s = 11$ % was tested in both cases. Equations for estimating f_g and f_f were borrowed from the literature. Specifically, for the smooth bed f_g was estimated by an equation reflecting the form of Eq. (7) while, for the rough bed, it was obtained using the Savat (1980) algorithm. The form resistance f_f was calculated by the equation proposed by Abrahams (1998), which coincides with Eq. (9) with $min\ (\pi/4, \Lambda) = \Lambda$, and $\Lambda = h/(D_r/2)$. Indeed, for $\Lambda < 1$ (i.e., when roughness elements protrude through the flow), which holds for both series of experiments, f is not affected by the elements' height, while it depends on their width. Changing k_s to D_r became always necessary when the roughness elements differ from hemispheres, for which $k_s = D_r$.

Equations for estimating f_w and f_m were developed from the fixed bed series and the mobile bed one, respectively. Together f_w and f_m accounted for almost 70 % of f, while f_g and f_f represented nearly 13 and 18 % of f. The analysis conducted to the following predictive equation of the friction factor for rough mobile beds:

$$f = f_g + f_f + f_m = \frac{8\tau_s}{\rho V_s^2} + \frac{16}{\pi}C_d\frac{h}{D_r}P + \frac{0.63}{F^2} \tag{23}$$

where τ_s is the surface shear stress and V_s is the calculated velocity provided by the Savat algorithm. Even if Eq. (23) results from a valuable methodology based on friction factor partitioning, its applicability is limited to the narrow experimental range.

The evaluation of the friction factor components was also performed by Abrahams and Parsons (1991), in a situation where only grain and form resistance were considered. The quantitative assessment of the two contributions assumed that they are additive. The grain resistance f_g was evaluated by the Savat (1980) algorithm, while the form resistance by subtracting f_g from f. They performed 73 overland flow experiments on 8 runoff plots situated on a gentle slope on gravel-covered desert pavement surfaces. The results pointed out that f can be well predicted by the Reynolds number and gravel concentration and size, and the best predictor was by far the gravel concentration. This implies that form resistance f_f was greater than grain resistance f_g, which was less than 10 % of f. This value is in line with that obtained by Hu and Abrahams (2006), while f_f is much greater, probably because f_f here implicitly embeds wave resistance f_w and bed-mobility resistance f_m. Abrahams and Parsons (1991) also highlighted that as grain resistance is often a minor component of total hydraulic resistance, in the light of the relation between shear stress and flow resistance, grain shear stress is also a small part of total shear stress. They also pointed out that into soil erosion models the sediment transport capacity varies with shear stress to a power greater than 1 but it is controlled, and should be modeled, by grain shear stress rather than total shear stress. Since the sediment transport capacity is largely controlled by rainfall and the rainfall effect declines for the deeper flows, according to the authors the distinction between grain and total shear stress should become relevant only for the deeper flows. In this case, grain shear stress must be used rather than total shear stress to accurately estimate the sediment transport capacity and avoiding large overestimation.

Nicosia et al. (2021b) calibrated Eq. (18) using the measurements performed by Liu et al. (2020) for five Chinese soils (Loessial, Cinnamon, Black, Red, and Purple soil) under equilibrium sediment transport. The results demonstrated that the proposed theoretical approach (Eqs. (12) and (18)) allowed for an accurate f estimate (Fig. 5). The scale factor a, which represents the soil effect on the Γ velocity profile parameter and flow resistance, increased with the transportability of soil particles,

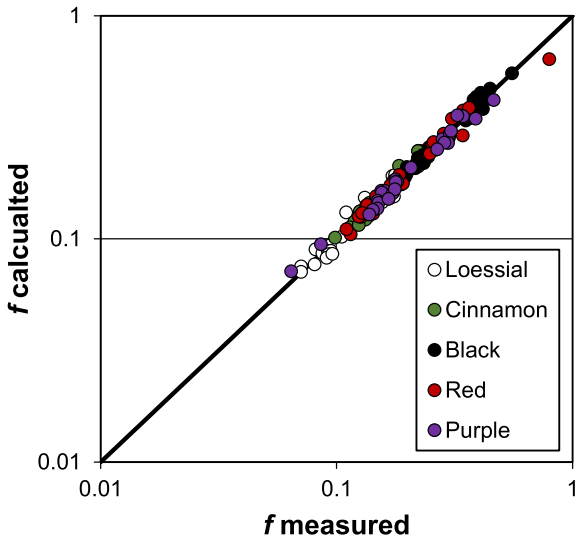

Fig. 5. Comparison between the measured and calculated values of the Darcy-Weisbach friction factor by Nicosia et al. (2021b) (Eqs. (12) and (18)).

which is associated with the reduction of both the flow energy required for sediment transport and the Darcy-Weisbach friction factor.

The theoretical flow resistance approach (Eqs. (12) and (18) with $d = 0$ and $m = 1$) was tested by Nicosia et al. (2022) using the literature measurements by Ali et al. (2012) and Zhang et al. (2011) carried out in sandy soils for both gentle (5–13 %) and steep (17–42 %) slopes. These two datasets refer to mobile bed flows in which the soil particle size is similar and the sediment load equates to the transport capacity. Therefore, in the absence of bed-forms and for given grain roughness, the effect of sediment transport on flow resistance is entirely accounted for the transport capacity. Eqs. (12) and (18) combined point out a direct relation between f and s. It is known (e.g., Zhang et al., 2011) that sediment transport capacity increases as a power function of slope gradient which, consequently, accounts for the effect of sediment transport on flow resistance. A single expression of the friction factor with a slightly varying (0.875–0.898) between gentle and steep slopes enabled good f predictions. Finally, overland flow resistance was greater on steep than on gentle slopes.

6. Concluding remarks and research needs

Hydraulic roughness is a key parameter for modeling shallow water flows and sheet erosion and is often expressed in terms of the Darcy-Weisbach friction factor. This factor primarily varies with roughness scale, with the inundation ratio and the Reynolds number controlling the friction mechanism for large and small-scale roughness conditions, respectively. For overland flows on smooth beds, rainfall intensity significantly affects flow resistance only in the laminar flow regime.

The analysis of the available literature on vegetation effects allows for concluding that flow resistance always increases with increasing the vegetation cover, but it does not change with vegetation type. For a given cover level, stems more efficiently control soil erosion than litter does. The studies regarding the effects of sediment transport lead to the conclusion that f (or its component due to sediment transport) increases with sediment concentration, slope, and Reynolds number, while it decreases with increasing values of Froude number and dimensionless sediment diameter.

Even though many studies are available in the literature and some conclusions are ascertained, some aspects must still be addressed, and some experimental conditions remain still unexplored.

The effects of rainfall intensity and sediment transport on overland flow resistance were less frequently investigated than the vegetation effect. A threshold I value (occurring in the range 32–95 mm h^{-1}), above which the influence on laminar flow occurs, should be identified. Moreover, the approach to evaluate the rainfall impact contribution to flow resistance (Δf), which is currently limited to fixed bed condition, could be extended to mobile bed condition. Although the investigated experimental ranges are generally quite wide, future studies concerning the rainfall effect on flow resistance should be carried out for steeper slopes. In addition, the simultaneous application of rainfall and inflow discharge for studying the effect of sediment transport would allow the reproduction of similar conditions to real ones.

One of the main tasks of overland flow hydraulics should be the deduction of the flow resistance law by integration of a known flow velocity distribution in the cross-section. While for the well and marginally inundated flows several studies (e.g., Bathurst, 1988; Nezu and Rodi, 1986; Ferro and Baiamonte, 1994; Carollo et al., 2002; Ferro, 2003; Shi et al., 2023) focused on velocity profile, this is not the case for the partially inundated flows as they are characterized by particularly shallow depths which impede the measurement of the local velocity by instruments like Acoustic Doppler Velocimeter. Thus, these types of overland flow (partially inundated) need advances on measurement techniques and theoretical framework.

The suggestion by Abrahams and Parsons (1991) of using grain shear stress rather than total shear stress for deeper flows has a major implication for sediment transport modeling and was confirmed in previous studies. However, either they did not provide a mathematical model to predict the single friction factor components (e.g., Pan et al., 2016; Ding et al., 2021) or focused on rangelands (Weltz et al., 1992). The friction factor partitioning model by Hu and Abrahams (2006), even though relied on a limited experimental range, is a valuable reference for future studies aimed at developing equations for predicting the overall friction factor from the individual components.

Declaration of competing interest

The authors declare that they have no known competing financial interests or personal relationships that could have appeared to influence the work reported in this paper.

Data availability

Data are available from original publications

Acknowledgements

All authors set up the research, analyzed and interpreted the results and contributed to write the paper. This research did not receive any specific grant from funding agencies in the public, commercial, or not-for-profit sectors.

References

Abrahams, A.D., 1998. Discussion: 'Macroscale surface roughness and frictional resistance in overland flow' by DSL Lawrence. Earth Surf. Process. Landf. 23, 857–859.

Abrahams, A.D., Parsons, A.J., 1991. Relation between infiltration and stone cover on a semiarid hillslope, southern Arizona. J.Hydrol. 122, 49–59.

Abrahams, A.D., Parsons, A.J., 1994. Hydraulics of interrill overland flow on stone-covered desert surfaces. Catena 23, 111–140.

Abrahams, A.D., Parsons, A.J., Luk, S.H., 1986. Resistance to overland flow on desert hillslopes. J. Hydrol. 88, 343–363.

Abrahams, A.D., Parsons, A.J., Wainwright, J., 1994. Resistance to overland flow on semiarid grassland and shrubland hillslopes, Walnut Gulch, southern Arizona. J. Hydrol. 156, 431–446.

Ali, M., Sterk, G., Seeger, M., Boersema, M., Peters, P., 2012. Effect of hydraulic parameters on sediment transport capacity in overland flow over erodible beds. Hydrol. Earth Syst. Sci. 16, 591–601.

Barenblatt, G.I., 1979. Similarity, Self-Similarity, and Intermediate Asymptotics. Consultants Bureau Plenum Press, New York and London, p. 218.

Barenblatt, G.I., 1987. Dimensional Analysis. Gordon & Breach, Science Publishers Inc., Amsterdam.

Barenblatt, G.I., 1991. On the scaling laws (incomplete self-similarity with respect to Reynolds numbers) for the developed turbulent flows in tubes. C.R. Acad. Sci. Ser. II 13, 307–312.
Barenblatt, G.I., 1993. Scaling laws for fully developed turbulent shear flows, part 1, basic hypothesis and analysis. J. Fluid Mech. 248, 513–520.
Bathurst, J.C., 1988. Velocity profile in high-gradient, boulder-bed channels. In: Proceedings of International Conference on Fluvial Hydraulics. IAHR, Budapest, pp. 29–34.
Bond, S., Kirkby, M.J., Johnston, J., Crowle, A., Holden, J., 2020. Seasonal vegetation and management influence overland flow velocity and roughness in upland grasslands. Hydrol. Process. 34 (18), 3777–3791.
Carollo, F.G., Ferro, V., Termini, D., 2002. Flow velocity measurement in vegetated channels. J. Hydraul. Eng. 128 (7), 664–673.
Carollo, F.G., Di Stefano, C., Nicosia, A., Palmeri, V., Pampalone, V., Ferro, V., 2021. Flow resistance in mobile bed rills shaped in soils with different texture. Eur. J. Soil Sci. 1–14.
Castaing, B., Gagne, Y., Hopfinger, E.J., 1990. Velocity probability density functions of high Reynolds number turbulence. Phys. D 46, 177–200.
Cen, Y., Zhang, K., Peng, Y., Rubinato, M., Liu, J., Ling, P., 2022. Experimental study on the effect of simulated grass and stem coverage on resistance coefficient of overland flow. Hydrol. Process. 36, e14705.
Dan, C., Liu, G., Zhao, Y., Shu, C., Shen, E., Liu, C., Tan, Q., Zhang, Q., Guo, Z., Zhang, Y., 2023. The effects of typical grass cover combined with biocrusts on slope hydrology and soil erosion during rainstorms on the Loess Plateau of China: an experimental study. Hydrol. Process. 37 (1), e14794.
De Marchi, G., 1977. Idraulica. vol. 2, U. Hoepli, Milano.
Di Stefano, C., Nicosia, A., Palmeri, V., Pampalone, V., Ferro, V., 2020. Flow resistance law under suspended sediment laden conditions. Flow Meas. Instrum. 74, 101771.
Di Stefano, C., Nicosia, A., Palmeri, V., Pampalone, V., Ferro, V., 2022. Rill flow velocity and resistance law: a review. Earth Sci. Rev. 231, 104092.
Ding, W., Li, M., 2016. Effects of grass coverage and distribution patterns on erosion and overland flow hydraulic characteristics. Environ. Earth Sci. 75, 477.
Ding, L., Fu, S., Zao, H., 2021. Hydraulic properties affected by litter and stem cover under overland flow. Hydrol. Process. 35, e14088.
Emmett, W.W., 1970. The hydraulics of overland flow on hillslopes: Dynamic and descriptive studies of hillslopes. Geol. Surv. Prof. Pap. A1–A67.
Ferro, V., 2003. Flow resistance in gravel-bed channels with large-scale roughness. Earth Surf. Process. Landf. 28, 1325–1339. https://doi.org/10.1002/esp.589.
Ferro, V., 2017. New flow resistance law for steep mountain streams based on velocity profile. J. Irrig. Drain. Eng. ASCE 143 (04017024), 1–6. https://doi.org/10.1061/(ASCE)IR.1943-4774.0001208.
Ferro, V., 2018. Assessing flow resistance in gravel bed channels by dimensional analysis and self-similarity. Catena 169, 119–127. https://doi.org/10.1016/j.catena.2018.05.034.
Ferro, V., 2020. Comment on "Overland runoff erosion dynamics on steep slopes with forages under field simulated rainfall and inflow by C. Li and C. Pan". Hydrol. Process. 34, 5505–5511. https://doi.org/10.1002/hyp.13938.
Ferro, V., Baiamonte, G., 1994. Flow velocity profiles in gravel-bed rivers. J. Hydraul. Eng. ASCE 120 (1), 60–80.
Ferro, V., Guida, G., 2022. A theoretically-based overland flow resistance law for upland grassland habitats. Catena 210, 105863.
Ferro, V., Porto, P., 2018. Applying hypothesis of self-similarity for flow resistance law in Calabrian gravel-bed rivers. J. Hydraul. Eng. ASCE 140 (04017061), 1–11. https://doi.org/10.1061/(ASCE)HY.1943-7900.0001385.
Gao, P., Abrahams, A.D., 2004. Bedload transport resistance in rough open-channel flows. Earth Surf. Process. Landf. 29 (4), 423–435.
Govers, G., 1992. Relationship between discharge, velocity and flow area for rills eroding loose, non –layered materials. Earth Surf. Process. Landf. 17, 515–528.
Govers, G., Takken, I., Helming, K., 2000. Soil roughness and overland flow. Agronomie 20 (2), 131–146. https://doi.org/10.1051/agro:2000114.
Guy, B., Dickinson, W., Rudra, R., 1987. The roles of rainfall and runoff in the sediment transport capacity of interrill flow. Trans. ASAE 30, 1378–1386.
Horton, R.E., 1945. Erosional development of streams and their drainage basins; hydrophysical approach to quantitative morphology. Bull. Geol. Soc. Am. 3, 340–349.
Hu, S., Abrahams, A.D., 2004. Resistance to overland flow due to bed-load transport on plane mobile beds. Earth Surf. Process. Landf. 29, 1691–1701.
Hu, S., Abrahams, A.D., 2005. The effect of bed mobility on resistance to overland flow. Earth Surf. Process. Landf. 30, 1461–1470.
Hu, S., Abrahams, A.D., 2006. Partitioning resistance to overland flow on rough mobile beds. Earth Surf. Process. Landf. 31, 1280–1291.
Jain, M.K., Kothyari, U.C., Ranga Raju, K.G., 2004. A GIS distributed rainfall-runoff model. J. Hydrol. 299, 107–135.
Katz, D.M., Watts, F.J., Burroughs, E.R., 1995. Effects of surface roughness and rainfall impact on overland flow. J. Hydraul. Eng. ASCE 121, 546–553.
Kim, J., Ivanov, V.Y., Katopodes, N.D., 2012. Hydraulic resistance to overland flow on surfaces with partially submerged vegetation. Water Resour. Res. 48, W10540. https://doi.org/10.1029/2012WR012047.
Lawrence, D.S.L., 1997. Macroscale surface roughness and frictional resistance in overland flow. Earth Surf. Process. Landf. 22 (4), 365–382.
Lawrence, D.S.L., 2000. Hydraulic resistance in overland flow during partial and marginal surface inundation: Experimental observations and modeling. Water Resour. Res. 36 (8), 2381–2393.
Li, C., Pan, C., 2020. Overland runoff erosion dynamics on steep slopes with forages under field simulated rainfall and inflow. Hydrol. Process. 34 (8), 1794–1809.
Li, P., Zhang, K., Wang, J., Meng, H., Nicosia, A., Ferro, V., 2022. Overland flow hydrodynamic characteristics in rough beds at low Reynolds numbers. J. Hydrol. 607, 127555.
Liu, C., Li, Z., Fu, S., Ding, L., Wu, G., 2020. Influence of soil aggregate characteristics on the sediment transport capacity of overland flow. Geoderma 369, 114338.
Mügler, C., Planchon, O., Patin, J., Weill, S., Silvera, N., Richard, P., Mouche, E., 2011. Comparison of roughness models to simulate overland flow and tracer transport experiments under simulated rainfall at plot scale. J. Hydrol. 402, 25–40.
Mutchler, C.K., Young, R.A., 1975. Soil detachment by raindrops. In: Present and Prospective Technology for Predicting Sediment Yield and Sources, ARS-S-40. USDA Science and Education Administration, Washington, DC, pp. 113–117.
Nearing, M.A., Kimoto, A., Nichols, M.H., Ritchie, J.C., 2005. Spatial patterns of soil erosion and deposition in two small, semiarid watersheds. J. Geophys. Res. 110, F04020.
Nearing, M.A., Polyakov, V.O., Nichols, M.H., Hernandez, M., Li, L., Zhao, Y., Armendariz, G., 2017. Slope–velocity equilibrium and evolution of surface roughness on a stony hillslope. Hydrol. Earth Syst. Sci. 21, 3221–3229.
Nezu, I., Rodi, W., 1986. Open-channel flow measurements with a Laser Doppler Anemometer. J. Hydraul. Eng. ASCE 112 (5), 335–355.
Nicosia, A., Di Stefano, C., Palmeri, V., Pampalone, V., Ferro, V., 2020a. Flow resistance of overland flow on a smooth bed under simulated rainfall. Catena 187, 104351.
Nicosia, A., Di Stefano, C., Pampalone, V., Palmeri, V., Ferro, V., Nearing, M.A., 2020b. Testing a theoretical resistance law for overland flow on a stony hillslope. Hydrol. Process. 1–9.
Nicosia, A., Di Stefano, C., Pampalone, V., Palmeri, V., Ferro, V., Polyakov, V., Nearing, M.A., 2020c. Testing a theoretical resistance law for overland flow under simulated rainfall with different types of vegetation. Catena 189, 104482.
Nicosia, A., Di Stefano, C., Pampalone, V., Palmeri, V., Ferro, V., 2021a. Testing a theoretically-based overland flow resistance law by Emmett's database. J. Hydrol. 603, 126862.
Nicosia, A., Di Stefano, C., Pampalone, V., Palmeri, V., Ferro, V., 2021b. Assessing an overland flow resistance approach under equilibrium sediment transport conditions. Catena 207, 105578.
Nicosia, A., Guida, G., Di Stefano, C., Pampalone, V., Ferro, V., 2022. Slope threshold for overland flow resistance on sandy soils. Eur. J. Soil Sci. 73, e13182.
Palmeri, V., Pampalone, V., Di Stefano, C., Nicosia, A., Ferro, V., 2018. Experiments for testing soil texture effects on flow resistance in mobile bed rills. Catena 171, 176–184.
Pan, C., Shangguan, Z., 2006. Runoff hydraulic characteristics and sediment generation in sloped grassplots under simulated rainfall conditions. J. Hydrol. 331, 178–185.
Pan, C., Ma, L., Wainwright, J., Shangguan, Z., 2016. Overland flow resistances on varying slope gradients and partitioning on grassed slopes under simulated rainfall. Water Resour. Res. 52, 2490–2512. https://doi.org/10.1002/2015WR018035.
Parsons, A.J., Abrahams, A.D., Wainwright, J., 1994. On determining resistance to interrill overland flow. Water Resour. Res. 30 (12), 3515–3521.
Phelps, H.O., 1975. Shallow laminar flows over rough granular surfaces. J. Hydraul. Div. 101 (3), 367–384.
Polyakov, V., Stone, J., Holifield Collins, C., Nearing, M.A., Paige, G., Buono, J., Gomez-Pond, R., 2018. Rainfall simulation experiments in the southwestern USA using the Walnut Gulch Rainfall Simulator. Earth Syst. Sci. Data 10, 19–26. https://doi.org/10.5194/essd-10-19-2018.
Roels, J.M., 1984. Flow resistance in concentrated overland flow on rough slope surfaces. Earth Surf. Process. Landf. 9 (6), 541–551.
Savat, J., 1977. The hydraulics of sheet flow on a smooth surface and the effect of simulated rainfall. Earth Surf. Process. 2, 125–140.
Savat, J., 1980. Resistance to flow in rough supercritical sheet flow. Earth Surf. Process. 5 (2), 103–122.
Shang, H., Zhang, K., Wang, Z., Yang, J., He, M., Pan, X., Fang, C., 2020. Effect of varying wheatgrass density on resistance to overland flow. J. Hydrol. 591, 125594.
Shen, H.W., Li, R., 1973. Rainfall effect on sheet flow over smooth surface. J. Hydraul. Div. ASCE 99, 771–792.
Shen, E., Liu, G., Jia, Y., Dan, C., Abd Elbasit, M.A.M., Liu, C., Gu, J., Shi, H., 2021a. Effects of raindrop impact on the resistance characteristics of sheet flow. J. Hydrol. 592, 125767. https://doi.org/10.1016/j.jhydrol.2020.125767.
Shen, E., Liu, G., Dan, C., Shu, C., Wang, R., Liu, X., Zhou, J., Chen, X., 2021b. Combined effects of rainfall and flow depth on the resistance characteristics of sheet flow on gentle slopes. J. Hydrol. 603, 127112. https://doi.org/10.1016/j.jhydrol.2021.127112.
Shen, E., Liu, G., Xia, X., Dan, C., Zheng, F., Zhang, Q., Zhang, Y., Guo, Z., 2023. Resistance to sheet flow induced by raindrop impact on rough surfaces. Catena 231, 107272.
Shi, H., Zhang, J., Huai, W., 2023. Experimental study on velocity distributions, secondary currents, and coherent structures in open channel flow with submerged riparian vegetation. Adv. Water Resour. 173, 104406. https://doi.org/10.1016/j.advwatres.2023.104406.
Smith, M.W., Cox, N.J., Bracken, L.J., 2007. Applying flow resistance equations to overland flows. Prog. Phys. Geogr. 31 (4), 363–387.
Sun, J., Fan, D., Yu, X., Li, H., 2018. Hydraulic characteristics of varying slope gradients, rainfall intensities and litter cover on vegetated slopes. Hydrol. Res. 49 (2), 506–516. https://doi.org/10.2166/nh.2017.097.
Takken, I., Govers, G., 2000. Hydraulics of interrill overland flow on rough, bare soil surfaces. Earth Surf. Process. Landf. 25, 1387–1402.
Toy, T.J., Foster, G.R., Renard, K.G., 2002. Soil erosion: Processes, Prediction, Measurement, and Control. John Wiley & Sons Inc, New York, USA.
Wang, L., Zhang, G., Wang, X., Li, X., 2018a. Hydraulics of overland flow influenced by litter incorporation under extreme rainfall. Hydrol. Process. 33, 737–747.

Wang, Y., Zhang, H., Yang, P., Wang, Y., 2018b. Experimental study of overland flow through rigid emergent vegetation with different densities and location arrangements. Water 10, 1638. https://doi.org/10.3390/w10111638.
Wang, J., Lv, X., Zhang, K., Li, P., Meng, H., 2019. Unsteady-state hydraulic characteristics of overland flow. J. Hydrol. Eng. 04019046.
Weltz, M.A., Awadis, A.B., Lane, L.J., 1992. Hydraulic roughness coefficients for native rangelands. J. Irrig. Drain. Eng. 118, 776–790.
Yalin, M.S., 1977. Mechanics of Sediment Transport. Pergamon Press, Oxford, U.K.
Yang, P.P., Zhang, H.L., Ma, C., 2017. Effects of simulated submerged and rigid vegetation and grain roughness on hydraulic resistance to simulated overland flow. J. Mt. Sci. 14 (10). https://doi.org/10.1007/s11629-016-4280-0.
Ye, C., Liu, X.N., Wang, X.K., 2015. Effects of roughness elements distribution on overland flow resistance. J. Mt. Sci. 12 (5), 1145–1156.
Yoon, Y.N., Wenzel, H.G., 1971. Mechanics of sheet flow under simulated rainfall. J. Hydraul. Div. ASCE 97, 1367–1385.
Zhang, G., Wang, L., Tang, K., Luo, R., Zhang, X.C., 2011. Effects of sediment size on transport capacity of overland flow on steep slopes. Hydrol. Sci. J. 56 (7), 1289–1299.
Zhang, K., Wang, Z., Wang, G., Sun, X., Cui, N., 2017. Overland-flow resistance characteristics of nonsubmerged vegetation. J. Irrig. Drain. Eng. 143 (8), 04017021-1.
Zhang, S., Zhang, J., Liu, Y., Liu, Y., Li, G., 2018. The resistance effect of vegetation stem diameter on overland runoff under different slope gradients. Water Sci. Technol. 78 (11), 2383–2391.
Zhang, S., Liu, Y., Wang, Z., Li, G., 2020. Effect of flexible vegetation lodging on overland runoff resistance. Water Environ. J. 34 (Supplement S1), 333–341.
Zhang, J., Zhang, S., Chen, S., Liu, M., Xu, X., Zhou, J., Wang, W., Ma, L., Wang, C., 2021. Overland flow resistance law under sparse stem vegetation coverage. Water 13, 1657.
Zhao, C., Gao, J., Huang, Y., Wang, G., Zhang, M., 2016. Effects of vegetation stems on hydraulics of overland flow under varying water discharges. Land Degrad. Dev. 27, 748–757.